

# Quantitative absorption tomography

Yoonjae Chung<sup>1,2,6</sup>, Sehyun Lee<sup>2,3</sup>, Herve Hugonnet<sup>2,3</sup>, Chulmin Oh<sup>2,3</sup>, Weisun Park<sup>2,3</sup>, Yeon Wook Kim<sup>4</sup>, Seung-Mo Hong<sup>4</sup>, YongKeun Park<sup>2,3,5\*</sup>

<sup>1</sup>Department of Electrical Engineering, KAIST, Daejeon, 34141, Republic of Korea

<sup>2</sup>KAIST Institute for Health Science and Technology, KAIST, Daejeon, 34141, Republic of Korea

<sup>3</sup>Department of Physics, KAIST, Daejeon, 34141, Republic of Korea

<sup>3</sup>Biomedical Research Center, Asan Institute for Life Sciences, Asan Medical Center, Seoul, Republic of Korea

<sup>4</sup>Department of Pathology, Asan Medical Center, University of Ulsan College of Medicine, Seoul 05505, Republic of Korea

<sup>5</sup>Tomocube Inc., Daejeon 34109, Republic of Korea

<sup>6</sup>Current affiliation: Department of Electrical Engineering, Stanford University, Stanford, CA 94305, United States

\*E-mail: [vk.park@kaist.ac.kr](mailto:vk.park@kaist.ac.kr)

## Abstract

Brightfield microscopy is central to wide range of biology, engineering, and histopathology; but is inherently limited to two-dimensional qualitative imaging, systematically investigating three-dimensional (3D) volumetric architecture. Here we introduce quantitative absorption tomography (QAT), a computational approach that quantitatively reconstructs high-resolution volumetric absorption coefficient distributions from brightfield focal stacks. By modeling absorption image formation in logarithmic intensity space and applying deconvolution with an absorption optical transfer function, QAT enables quantitative, spectrally resolved 3D absorption imaging without interferometry, sample rotation, or specialized hardware. We validate QAT using spectrally selective phantoms and demonstrate absorption-specific contrast complementary to refractive index tomography in living melanocytes and intact plant tissue. QAT further scales to millimeter-scale volumes of H&E-stained human tissue, revealing 3D histological microarchitecture without serial sectioning. This approach extends brightfield microscopy toward practical 3D histopathology.

## Introduction

Brightfield microscopy remains one of the most widely used imaging modalities in biology and medicine owing to its simplicity, robustness, and compatibility with chromogenic stains<sup>1</sup>. In particular, histopathology based on hematoxylin and eosin (H&E) staining and brightfield microscopy constitutes the gold standard for disease diagnosis and guides clinical decision-making across a broad range of conditions. Despite its central role, conventional brightfield microscopy is fundamentally limited to two-dimensional (2D) observation of thin tissue sections, typically 4–5  $\mu\text{m}$  thick. Moreover, standard brightfield imaging provides only qualitative, 2D absorption contrast, inferred from transmitted intensity normalized by uniform illumination, rather than quantitative measurements of the absorption coefficient. As a result, critical three-dimensional (3D) structural information remains largely inaccessible in a systematic and quantitative manner<sup>2–4</sup>.

Recovering volumetric information from biological specimens has long been a goal of optical microscopy. One widely adopted approach is serial sectioning followed by digital reconstruction, but this process is labor-intensive, destructive, and prone to section loss, distortion, and alignment errors<sup>5</sup>. Optical alternatives, including fluorescence-based volumetric imaging and tissue clearing combined with light-sheet microscopy<sup>6</sup>, enable high-resolution 3D visualization but require specialized labeling, sample preparation, and instrumentation that are not routinely available in clinical pathology workflows<sup>7</sup>. Moreover, fluorescence contrast differs fundamentally from chromogenic absorption contrast, complicating direct comparison with established histological standards.

Several optical strategies have sought to extend brightfield microscopy into three dimensions. Optical projection tomography and related methods reconstruct volumetric attenuation by acquiring angular projections<sup>8,9</sup>, but typically require sample rotation or optical clearing and suffer from resolution trade-offs at high numerical apertures. Other approaches improve axial sectioning through computational deconvolution of brightfield focal stacks<sup>10,11</sup>, yet these methods are often qualitative and limited to serial ultrathin sections. Furthermore they do not yield quantitative absorption coefficients or spectral separation<sup>11–13</sup>. As a result, a general, quantitative framework for 3D absorption imaging compatible with standard brightfield microscopes has been lacking.

A number of label-free optical techniques have been proposed to infer 3D tissue structure without serial sectioning. Holotomography, a 3D quantitative phase imaging technique, reconstruct the refractive index (RI) distribution of thick specimens, exploiting RI as an intrinsic imaging contrast<sup>14,15</sup>. While powerful for transparent objects, these approaches rely on indirect inference of chromogenic contrast and require careful validation against ground truth. In contrast, direct 3D imaging of optical absorption—the physical origin

of contrast in brightfield histology—has remained comparatively underexplored.

While these approaches improve axial sectioning or provide volumetric information, they largely treat brightfield contrast as a qualitative attenuation signal or rely on indirect inference of chromogenic contrast. In contrast, QAT introduces a distinct imaging paradigm by explicitly modeling optical absorption as the primary contrast mechanism and reconstructing 3D absorption coefficients through a physics-based inverse model.

Here, we introduce QAT, a computational framework that reconstructs 3D absorption (extinction) coefficient distributions from conventional brightfield focal stacks. The central insight of QAT is that, under weak-scattering conditions, absorption can be modeled as a linear imaging process when expressed in logarithmic intensity space. This formulation enables computation of an absorption optical transfer function (OTF) and its inversion via deconvolution, yielding quantitative volumetric absorption maps without interferometry, coherent illumination, or sample rotation. In its simplest implementation, QAT requires only standard Köhler illumination and axial scanning, making it compatible with existing brightfield microscope platforms.

We demonstrate its applicability across a wide range of specimens and length scales. Using spectrally selective absorption phantoms, we validate accurate 3D localization and wavelength-specific absorption reconstruction. We show that QAT provides absorption-specific contrast that complements RI tomography in pigment-containing cells and enables long-term, label-free monitoring of melanogenesis in living melanoma cells. We further extend QAT to *in vivo* imaging of intact *Petunia hybrida* petal cells, resolving endogenous pigment distributions in optically complex plant tissue. Finally, we apply QAT to large-area, H&E-stained human pancreatic tissue sections, demonstrating millimeter-scale volumetric absorption imaging with submicron resolution. By enabling quantitative, 3D absorption imaging using brightfield microscopy, QAT bridges a critical gap between conventional brightfield imaging and volumetric optical imaging. This approach offers a practical pathway toward 3D biology, histopathology, and spatial analysis of stained and pigmented specimens using familiar imaging workflows.

## Results

### Quantitative absorption tomography: theory

Microscopic image formation can be described by the interaction of a complex RI distribution  $n$  of a sample  $\bar{n}(x, y, z) = n(x, y, z) + i\kappa(x, y, z)$  with an illumination. The real RI values  $n$  describes light refraction (locally changing illumination's phase) while the imaginary RI  $\kappa$ , the extinction coefficient relates to light absorption (locally changing illumination's strength). Under the assumption of a weakly scattering object, a linear relation between the measured image intensity attenuation  $S = \log[I(\mathbf{r})/I_0(\mathbf{r})]$  and the object complex RI values can be derived<sup>16</sup>:

$$S = H_A * V_{imag} + H_P * V_{real},$$

where  $V_{imag}$  and  $V_{real}$  are the imaginary and real parts of the scattering potential  $V = (2\pi/\lambda)^2[\bar{n}^2(\mathbf{r}) - n_0^2]$ ,  $\lambda$  is the wavelength and  $n_0$  is the surrounding background RI. Under the weak scattering condition ( $\bar{n} - n_0 \ll 1$ ), the extinction coefficient and RI are proportional to the imaginary and real part of the scattering potential  $\kappa \cong \frac{V_{imag}}{8\pi^2/\lambda^2 n_0}$  and  $n \cong \frac{V_{real}}{8\pi^2/\lambda^2 n_0}$  making reconstruction of either quantity equivalent.

$H_A$  and  $H_P$  are the absorption and phase transfer function of the microscope which can be computed from the pupil plane intensity distribution  $\rho$  as<sup>17</sup>,

$$H_P = -128\pi^4 \text{Im}[G^* \mathcal{F}^{-1}\{\tilde{G}k_z\rho\}],$$

$$H_A = -128\pi^4 \text{Re}[G^* \mathcal{F}^{-1}\{\tilde{G}k_z\rho\}],$$

where  $k_z$  is the axial wavevector component,  $\mathcal{F}$  the Fourier transform and the tilde  $\sim$  denotes Fourier transformed quantities. The extinction and refractive index images of the sample are obtained through deconvolution of the microscope intensity stack by the transfer function.

To separate the contribution of  $V_{imag}$  and  $V_{real}$  at least two measurements  $S_i$  with different illuminations  $\rho_i$  are needed and image formation is expressed with a matrix equation<sup>18</sup>.

$$\tilde{\mathbf{S}} = \begin{pmatrix} \tilde{S}_1 \\ \tilde{S}_2 \\ \dots \end{pmatrix} = \begin{pmatrix} \tilde{H}_{A1} & \tilde{H}_{P1} \\ \tilde{H}_{A2} & \tilde{H}_{P2} \\ \dots & \dots \end{pmatrix} \begin{pmatrix} \tilde{V}_{imag} \\ \tilde{V}_{real} \end{pmatrix} = \tilde{\mathbf{H}} \tilde{\mathbf{V}},$$

which is solved by Weiner deconvolution with regularization  $\alpha$ :

$$\tilde{\mathbf{V}} = (\tilde{\mathbf{H}}\tilde{\mathbf{H}}^\dagger + \alpha)^{-1}\tilde{\mathbf{H}}^\dagger\tilde{\mathbf{S}}.$$

When  $V_{real}$  is not of interest, one can instead determine  $V_{imag}$  with a single illumination if  $H_p = 0$ . This condition is met for an illumination  $\rho = 1/k_z$  since  $G^*\mathcal{F}^{-1}\{\tilde{G}k_z\rho\} = |G|^2$  resulting in  $H_p = 0$ .

The separation of  $\kappa$  and  $n$ , i.e., the separation of  $V_{imag}$  and  $V_{real}$ , can be formulated as a linear inverse problem, in which intensity stacks acquired under distinct illumination conditions provide independent measurements with different absorption and phase transfer functions. In this framework, the sufficiency of the illumination scheme is determined by the linear independence of the corresponding transfer functions within the spatial-frequency band of interest. The structured illumination patterns used here provide distinct and complementary sampling of spatial frequencies, resulting in a well-conditioned forward operator for joint reconstruction of  $\kappa$  and  $n$  within the intended resolution range.

Unlike conventional brightfield deconvolution approaches that aim to suppress out-of-focus blur without assigning physical meaning to the reconstructed intensity, QAT explicitly links the reconstructed volume to the absorption coefficient through a quantitative inverse model derived from 3D transfer function theory.

### Quantitative absorption tomography: experimental validation

To experimentally validate QAT, we implemented a programmable brightfield microscopy system and employed spectrally selective absorption phantoms that provide a well-defined ground truth. While QAT relies on through-focus stack acquisition and computational deconvolution, its key distinction lies in reconstructing quantitative absorption coefficients by explicitly computing the point spread function from 3D OTF theory, accounting for both refraction and absorption effects<sup>20,21</sup>. Although joint reconstruction of phase and absorption has been demonstrated within quantitative phase imaging (QPI) frameworks<sup>22,23</sup>, direct, quantitative, and color-resolved 3D absorption imaging of stained specimens has remained comparatively unexplored.

In our implementation (Fig. 1a), programmable angular illumination was achieved using a digital micromirror device (DMD) positioned at the condenser pupil plane. The DMD projected sequential illumination patterns under red (624 nm), green (520 nm), and blue (455 nm) LED illumination, while transmitted light was collected by a high-numerical-aperture objective. Axial scanning of the sample generated wavelength-resolved brightfield focal stacks encoding both in-focus and out-of-focus absorption contributions. For absorption-only QAT, multiple illumination patterns were aggregated to form an effective partially coherent Köhler illumination, enabling reconstruction using a single composite absorption transfer function.

Representative DMD-generated pupil illumination patterns are shown in Fig. 1b. These patterns collectively fill the condenser aperture and approximate standard brightfield illumination while maintaining compatibility with multi-illumination acquisition schemes used for joint phase-absorption imaging. Under this illumination, raw brightfield focal stacks exhibit pronounced axial blur, diffraction artifacts, and wavelength-dependent cross-talk. Absorbing structures appear axially elongated, and their apparent color varies with defocus, illustrating the fundamental limitations of conventional brightfield imaging for volumetric absorption analysis.

To quantitatively evaluate the performance of QAT, we imaged a mixture of cyan, magenta, and yellow (CMY) laser printer toner particles, which selectively absorb red, green, and blue light, respectively. This sample serves as a spectrally orthogonal absorption phantom with well-defined wavelength specificity. Following deconvolution of the logarithmic intensity stacks using wavelength-specific absorption transfer functions, QAT reconstructs three-dimensional absorption volumes with strong suppression of out-of-focus background and accurate spatial localization.

Orthogonal slices demonstrate that individual particles are sharply confined along the axial direction, with minimal elongation compared to the raw brightfield data. Importantly, QAT preserves spectral selectivity: cyan, magenta, and yellow particles are correctly assigned to their respective absorption channels, with negligible axial color bleed-through. These results demonstrate that QAT not only enhances axial sectioning but also faithfully recovers wavelength-dependent absorption contrast in three dimensions.

These experimental results establish QAT as a physically accurate and robust framework for 3D absorption imaging using brightfield microscopy. By combining programmable illumination, focal-stack acquisition, and absorption-aware deconvolution, QAT enables quantitative, spectrally resolved volumetric reconstruction of absorbing specimens—capabilities that are not accessible with conventional two-dimensional brightfield imaging.

Although multi-illumination QAT enables simultaneous reconstruction of refractive index and absorption with optimized transfer functions and aberration correction (Fig. 1c), absorption-only QAT can be performed using aggregated illumination patterns without angular diversity. In this mode, all measurements were acquired using eight sequential DMD-generated pupil patterns that were

combined to form a single effective brightfield pupil. This strategy improves robustness to pattern-to-pattern intensity fluctuations and noise while maintaining consistency with acquisition protocols used for joint phase–absorption reconstructions in live-cell experiments.

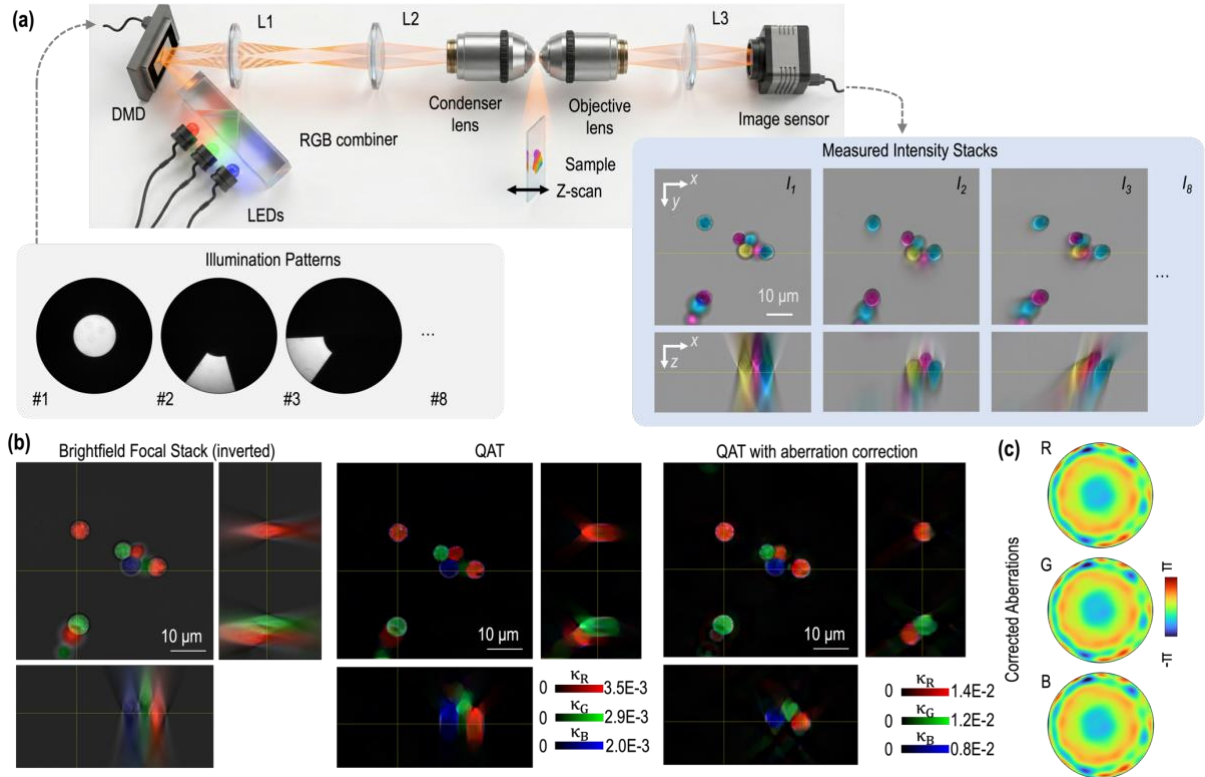


**Figure 1 | Principle and validation of QAT.** (a), Optical implementation. A DMD placed at the condenser pupil sequentially projects programmed illumination patterns under red (624 nm), green (520 nm), and blue (455 nm) LED illumination. Transmitted light is collected by a high-NA objective, and through-focus intensity stacks are recorded by axial scanning of the sample. (inset left), Representative pupil illumination patterns generated by the DMD (three shown out of 8), which together form an effective partially coherent brightfield illumination for absorption reconstruction. (inset, right), Measured RGB brightfield focal stacks acquired at different axial positions ( $I_1$ – $I_3$  shown). (b) QAT reconstruction results for a mixture of cyan, magenta, and yellow (CMY) laser printer toner particles, which selectively absorb red, green, and blue light, respectively. (c) The corrected pupil aberration patterns at the red, green, and blue.

In this work, we employ both modes depending on the application. Multiple structured illuminations are used to jointly reconstruct refractive index and absorption in live-cell experiments, while absorption-only QAT is adopted for large-area imaging of stained tissue to maximize robustness and throughput. In all cases, reconstructed extinction coefficient volumes are further refined using total variation regularization with channel-specific weights ( $\lambda_{TV,R} = 0.001$ ,  $\lambda_{TV,G} = 0.004$ ,  $\lambda_{TV,B} = 0.001$ ) with non-negativity constraints<sup>19</sup>, improving noise robustness while preserving sharp axial sectioning.

## Quantitative absorption tomography of live unlabeled melanocytes

Melanocytes constitute a unique and biologically important cell type characterized by the presence of melanin, a strongly absorbing endogenous pigment with central roles in pigmentation, photoprotection, and disease. Unlike most mammalian cells, melanocytes exhibit a high and spatially heterogeneous optical absorption due to melanin synthesis, transport, and aggregation. This pathophysiologically important pigment makes melanocytes an ideal—but previously challenging—target for 3D absorption imaging.

In conventional brightfield microscopy, melanin-containing regions are visible as dark features; however, the observed contrast represents a mixture of absorption, phase retardation, and out-of-focus contributions. Representative brightfield focal stacks of melanocytes (Fig. 2a, left column) illustrate this limitation: melanin appears axially elongated, its depth distribution is ambiguous,

and its apparent morphology varies with focus position. As a result, conventional brightfield imaging does not allow quantitative or 3D interpretation of intracellular melanin organization.

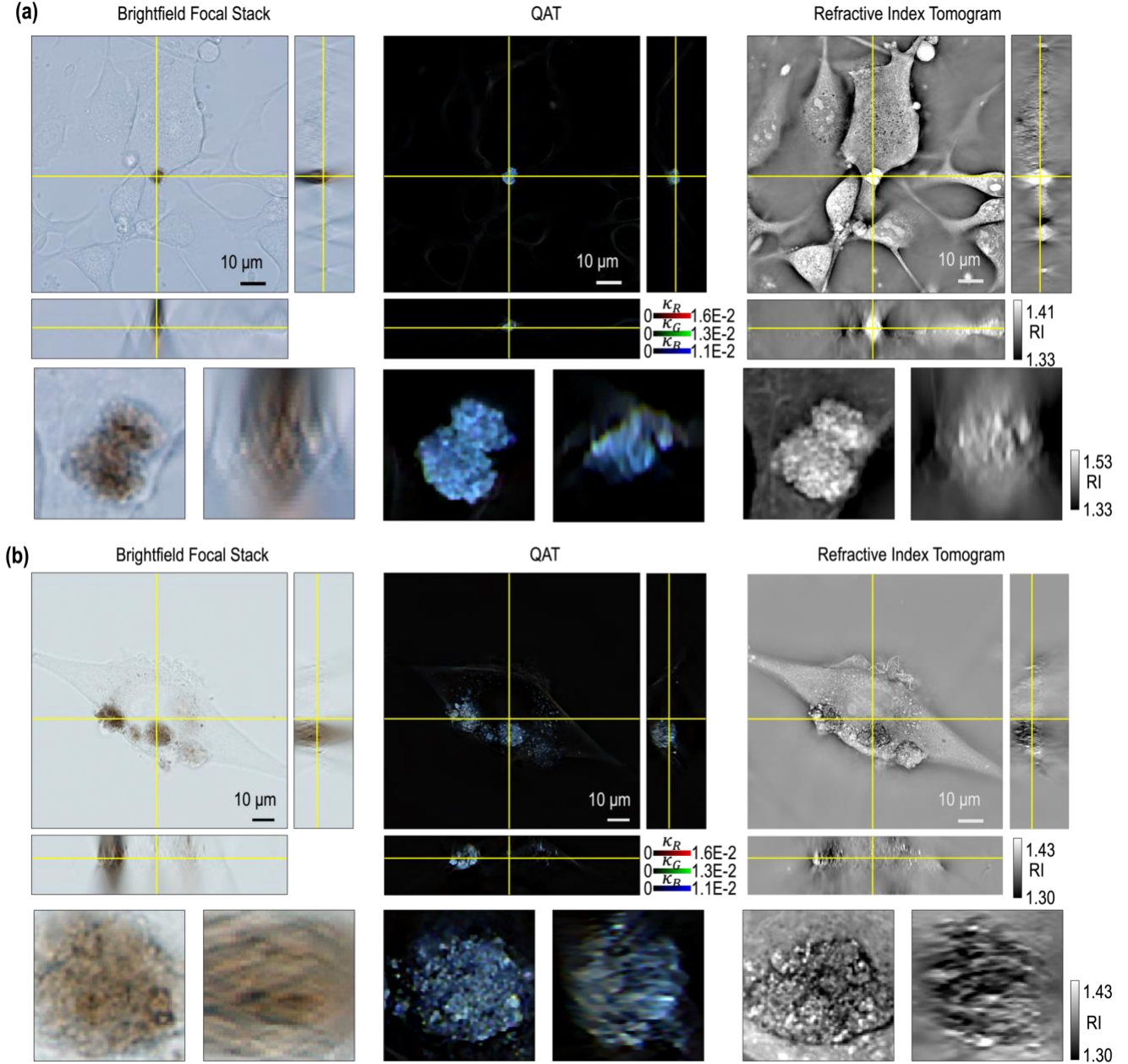


Figure 2 | Quantitative absorption tomography of melatocytes. (a) representative cells with sparse intracellular pigment. Left column: Raw brightfield images. Middle column: QAT reconstructions provide enhanced axial sectioning and accurate 3D localization of absorbing structures. Orthogonal slices (x-y, x-z, and y-z; yellow crosshairs) highlight the volumetric distribution of pigment with strong suppression of out-of-focus background. Right column: Corresponding RI tomograms of the same cells reveal overall cellular morphology but lack specificity to pigment accumulation, underscoring the complementary contrast provided by absorption imaging. (b) cells with dense pigment aggregates. Insets display zoomed views of reconstructed absorption volumes, emphasizing subcellular pigment organization.

QAT reconstruction of the extinction coefficient fundamentally changes this picture (Fig. 2a, middle column). By isolating absorption-specific contrast and suppressing out-of-focus background, QAT recovers the true 3D distribution of melanin within individual

melanocytes. Orthogonal slices reveal sharply confined absorption signals corresponding to melanin-rich subcellular regions, enabling accurate depth localization and volumetric mapping. Melanin aggregates can be traced continuously across axial planes, providing direct access to their spatial organization within the cell.

For comparison, RI tomograms reconstructed from the same datasets are shown in Fig. 2a (right column). RI imaging clearly delineates overall cellular morphology, including cell boundaries and organelle-rich regions, but does not selectively highlight melanin. Melanocytes with sparse and dense melanin content appear similar in RI contrast, underscoring a limitation of phase-based imaging for studying pigment biology. In contrast, QAT directly measures optical absorption and thus provides chemically specific contrast for melanin, independent of surrounding cellular morphology.

Figure 2b further highlights the ability of QAT to capture heterogeneous melanocyte states. Cells with sparse melanin exhibit localized absorption confined to small intracellular domains, whereas heavily pigmented melanocytes display dense, volumetric absorption distributions. In both cases, QAT preserves axial resolution and contrast across a wide dynamic range of absorption strength, demonstrating robustness to the extreme optical heterogeneity characteristic of melanocytes.

### Live-cell monitoring of melanogenesis using QAT

A major advantage of QAT is its ability to image endogenous absorbers without exogenous labels, enabling long-term live-cell measurements with minimal perturbation or phototoxicity. We leveraged this label-free capability to perform time-lapse, 3D monitoring of melanogenesis in living melanocytes, a dynamic process driven by the synthesis, transport, and redistribution of melanin. We applied QAT to B16-BL6 murine melanoma cells undergoing forskolin-induced melanogenesis and acquired volumetric datasets over a 24 h period (Fig. 3). This label-free configuration avoids photobleaching, phototoxicity, and molecular interference, which commonly limit long-term fluorescence-based studies of pigment biology.

Representative brightfield images acquired at successive time points are shown in Fig. 3. Although melanin-containing regions appear as dark features, brightfield images suffer from mixed phase-absorption contrast and strong axial blur, obscuring both the 3D organization of melanin and its temporal evolution. As a result, identifying melanogenic cells and tracking pigment dynamics over time remains challenging using brightfield microscopy alone.

QAT absorption reconstructions reveal a fundamentally different view of melanogenesis (Fig. 3, second and third rows). Absorption maximum-intensity projections and axial slices show the gradual emergence of localized absorption signals in a subset of cells, corresponding to melanin accumulation. Over time, these absorption signals intensify and spatially expand, revealing melanin redistribution along dendritic extensions. These observations are consistent with known melanosome transport processes and demonstrate that QAT enables direct, 3D visualization of melanin dynamics in living cells.

Simultaneously reconstructed RI tomograms (Fig. 3, third row) provide high-contrast visualization of overall cell morphology and proliferation toward confluence. However, RI contrast alone does not distinguish melanogenic cells from non-melanogenic neighbors, underscoring the limited functional specificity of phase-based imaging for pigment-related processes. In contrast, QAT selectively highlights melanin through absorption contrast, enabling clear discrimination between pigment-producing and non-producing cells within the same population.

Overlaying QAT absorption maps on RI tomograms (Fig. 3, fourth row) highlights the complementary nature of the two contrasts. Absorption signals are confined to melanin-rich subcellular regions, while RI maps provide the surrounding cellular context. Magnified views further reveal subcellular-scale pigment aggregation, transport, and reorganization over time, emphasizing the ability of QAT to resolve dynamic absorption-driven processes in three dimensions.

All live-cell experiments were performed using incoherent LED illumination at low irradiance (1.3 mW/cm<sup>2</sup> measured at the sample plane) and sparse temporal sampling. The total optical dose delivered over the 24 h acquisition was substantially lower than that typically used in fluorescence time-lapse imaging. Under these conditions, we observed no detectable photobleaching, morphological abnormalities, or growth arrest, indicating minimal phototoxic perturbation.

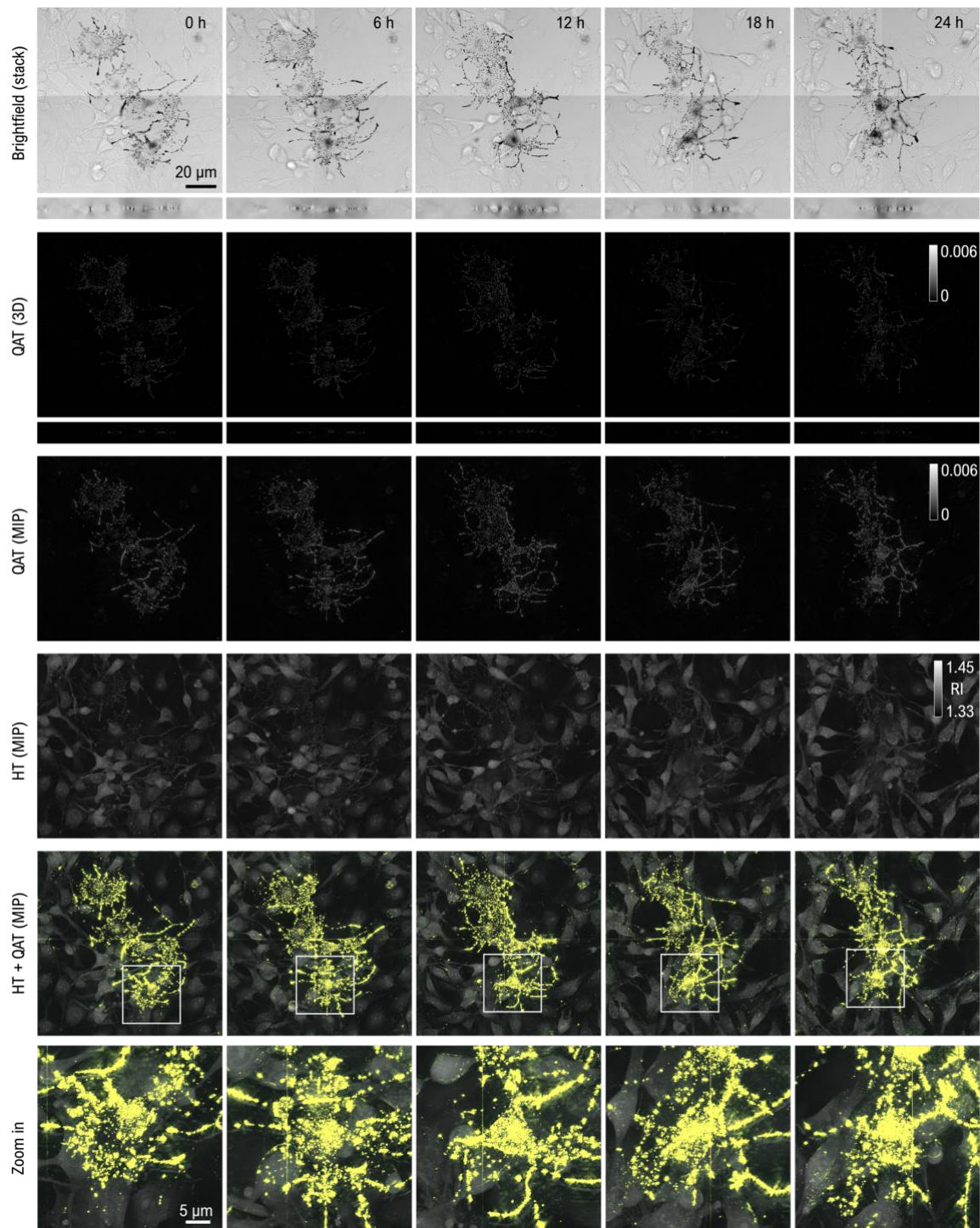


**Figure 3 | Live-cell quantitative absorption tomography reveals dynamic melanogenesis in melanoma cells.** Time-lapse imaging of forskolin-induced melanogenesis in living B16-BL6 melanoma cells over 24 h using quantitative absorption tomography (QAT). Top row: Representative brightfield images at successive time points show weak contrast and substantial axial blur, limiting visualization of pigment dynamics. Second row: Corresponding QAT absorption maximum-intensity projections (MIPs) reveal the emergence and redistribution of melanin-associated absorption with high specificity and reduced background. Third row: RI tomograms of the same field of view capture overall cell morphology and proliferation but do not distinguish pigment-producing cells. Fourth row: Overlay of QAT absorption (yellow) on RI maps (grayscale) highlights selective melanin accumulation in a subset of cells, primarily along dendritic extensions. Bottom row: Magnified views of the boxed regions illustrate subcellular-scale pigment transport, aggregation, and spatial reorganization over time. QAT enables stable, label-free monitoring of intracellular pigment dynamics over long durations, revealing heterogeneous melanogenic responses that are not discernible from phase-based contrast alone.

## In vivo volumetric absorption imaging of living *Petunia hybrida* petal cells

To demonstrate the applicability of QAT beyond animal cells and into plant biology, we performed *in vivo*, time-lapse 3D absorption imaging of living *Petunia hybrida* petal cells in quantitative manners. Plant petals represent optically complex, pigment-rich tissues containing multiple endogenous chromophores whose spatial organization and dynamics are central to plant physiology, yet remain challenging to visualize in three dimensions under native conditions.

We imaged intact *Petunia hybrida* petals while the flower remained attached to the living plant (Fig. 4a). A single petal was gently positioned between two coverslips on the microscope stage, and hydration was maintained throughout the experiment to preserve physiological viability and RI matching. This minimally invasive configuration enabled repeated acquisition of volumetric brightfield focal stacks over time without chemical fixation, labeling, or detachment of the tissue from the organism.

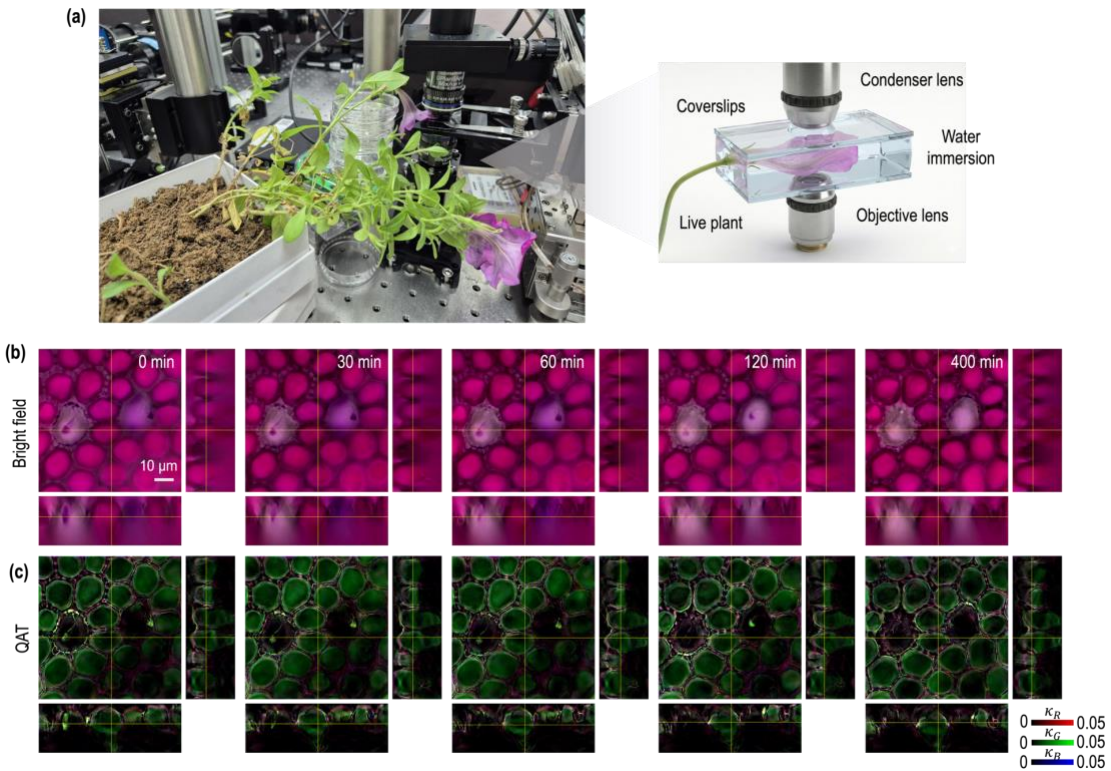


**Figure 4 | In vivo quantitative absorption tomography of living *Petunia hybrida* petal cells.** (a) Experimental configuration for *in vivo* imaging of living *Petunia hybrida* petal cells. The flower remains attached to the plant, while a single petal is gently positioned between coverslips on the microscope stage. (inset) Schematic of the transmission-mode imaging geometry used for volumetric absorption reconstruction. (b) RGB QAT absorption reconstructions of petal epidermal cells shown as orthogonal slices (x–y, x–z, and y–z; yellow crosshairs). Vacuolar pigment absorption is resolved throughout the tissue thickness with strong axial sectioning. Color-composite absorption volumes reveal cell-to-cell heterogeneity and the 3D organization of pigment-filled vacuoles, which are not discernible in conventional two-dimensional brightfield imaging. QAT enables label-free, volumetric absorption imaging of intact, living plant tissue under minimally invasive conditions..

Raw brightfield focal stacks exhibit strong axial blur and limited depth discrimination, obscuring the 3D organization of epidermal cells and their intracellular pigment pools (Fig. 4b, top row). In contrast, QAT reconstruction yields high-resolution, RGB absorption volumes that clearly resolve individual epidermal cells and their pigment-filled vacuoles throughout the tissue thickness (Fig. 4b, bottom row). Orthogonal reveal sharply localized absorption signals, demonstrating effective axial sectioning in an optically heterogeneous, living plant tissue.

The reconstructed absorption volumes further reveal the 3D distribution of multiple endogenous pigments within the petal cells. Distinct spectral signatures across the red, green, and blue channels are consistent with the presence of different classes of petal pigments, including anthocyanin-type vacuolar pigments. Color-composite renderings highlight pronounced cell-to-cell variability in pigment content and spatial arrangement, features that are not accessible using conventional two-dimensional brightfield microscopy.

Importantly, time-lapse QAT imaging captures dynamic changes in pigment organization within living petal cells. Over successive

time points, we observed gradual redistribution of pigment pools in a subset of cells, manifested as changes in the 3D shape and extent of absorption regions. These observations demonstrate that QAT enables longitudinal, label-free monitoring of pigment dynamics in living plant tissue, providing access to spatiotemporal information that is difficult to obtain with fluorescence-based or phase-based approaches.

### Large-scale 3D absorption imaging of H&E-stained human tissue

H&E staining has been the cornerstone of histopathology for more than a century. Hematoxylin selectively stains cell nuclei, while eosin highlights cytoplasmic and extracellular components, together providing a powerful and intuitive visualization of tissue architecture. Despite its central role in clinical diagnosis, H&E-based pathology has remained fundamentally limited to qualitative, two-dimensional assessment of thin tissue sections, relying heavily on visual interpretation by pathologists. To overcome these limitations, we applied QAT to formalin-fixed, paraffin-embedded (FFPE) human pancreatic tissue sections stained with H&E, enabling volumetric, quantitative absorption imaging of standard histological specimens. Unlike conventional brightfield microscopy, which integrates out-of-focus contributions along the optical axis, QAT reconstructs the 3D distribution of absorption coefficients, directly corresponding to hematoxylin- and eosin-associated pigments.

Representative orthogonal slices from raw brightfield focal stacks and corresponding QAT reconstructions are shown in Fig. 5a. In conventional brightfield images, nuclear and cytoplasmic features appear axially blurred due to strong out-of-focus contributions, limiting depth discrimination and obscuring fine 3D structure. In contrast, QAT markedly suppresses axial blur and resolves sharply localized absorption contrast throughout the tissue thickness. Hematoxylin-rich nuclei and eosin-stained cytoplasmic regions exhibit distinct, wavelength-dependent absorption signatures, enabling clear separation and 3D localization of nuclear and cytoplasmic components.

3D renderings of the reconstructed absorption volumes (Fig. 5b,c) reveal tissue microarchitecture across tens of microns in depth, including glandular organization, stromal structures, and subcellular features that are difficult or impossible to assess in two-dimensional sections. Notably, QAT resolves high-resolution subcellular absorption patterns within nuclei and cytoplasm, demonstrating that standard H&E staining contains rich 3D information that has remained largely inaccessible using conventional microscopy.

To evaluate scalability, we performed tiled QAT imaging and reconstructed a millimeter-scale absorption volume from a large-area pancreatic tissue section (Fig. 5d). The stitched volume preserves submicron lateral and axial resolution across the entire field of view, maintaining consistent spectral absorption contrast across tiles. Representative subregions illustrate diverse tissue architectures, including nuclear-dense regions, fibrous stroma, and eosin-rich cytoplasmic domains, all visualized with enhanced axial sectioning and spectral fidelity compared to conventional brightfield images.

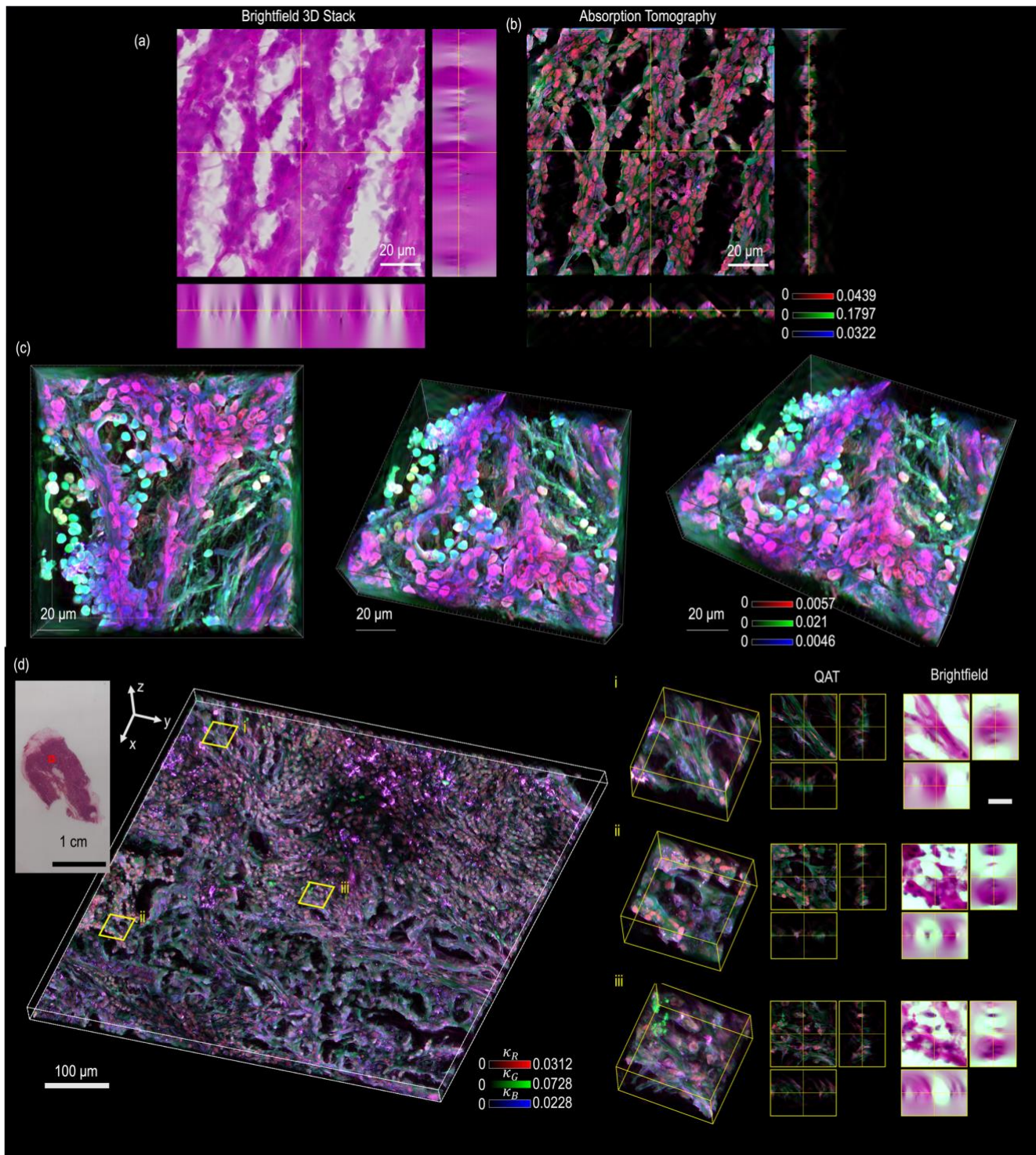


**Figure 5 | Large-scale 3D absorption imaging of H&E-stained human tissue using QAT.** **a-b**, Representative orthogonal slices from conventional brightfield focal stacks (a) and corresponding RGB QAT absorption reconstructions (b) of an H&E-stained human pancreatic tissue section. **c**, 3D maximum-intensity-projection (MIP) renderings of the reconstructed absorption volume, shown from different viewing angles, revealing volumetric organization of tissue microarchitecture. **d**, Large-area stitched QAT volume covering a millimeter-scale tissue region (left; inset shows macroscopic photograph of the section). Three representative subvolumes (i–iii) are highlighted and compared with corresponding conventional brightfield (BF) images (right). QAT preserves spectral absorption contrast and fine structural detail across scales, whereas BF images remain dominated by axial blur.

## Discussions

A key conceptual advance of QAT lies in recognizing that optical absorption, unlike phase contrast, can be treated as a linear imaging process under weak-scattering conditions when expressed in logarithmic intensity space. This formulation allows the absorption OTF to be analytically computed and inverted, yielding quantitative 3D extinction coefficient distributions. Importantly, QAT does not rely on interferometry, coherent illumination, or sample rotation, making it inherently compatible with widely used brightfield microscope architectures.

Beyond this conceptual framework, we demonstrated that a DMD-based multi-illumination scheme enables optimization of the 3D OTF for high-quality reconstruction of both absorption and refractive index tomograms. By analyzing intensity image stacks acquired under multiple illumination patterns, we further extracted wavelength-dependent pupil aberration patterns of the imaging system and digitally corrected them during reconstruction. This combined strategy enables high-fidelity volumetric imaging that would be difficult to achieve with conventional brightfield setups.

Our results show that QAT provides effective axial sectioning and spectral specificity that are not accessible with conventional brightfield imaging. Validation experiments using spectrally selective CMY toner particles (Fig. 1) confirmed accurate 3D localization and faithful recovery of wavelength-dependent absorption contrast, establishing QAT as a quantitative imaging modality rather than a contrast-enhancement technique.

At the cellular level, QAT reveals absorption-specific information that is fundamentally complementary to refractive index tomography. Experiments on pigment-containing cells (Fig. 2) and live-cell melanogenesis (Fig. 3) highlight an intrinsic asymmetry between phase-based and absorption-based imaging. While refractive index contrast effectively captures overall cellular morphology, it lacks chemical specificity for chromogenic or pigmented structures. In contrast, absorption contrast directly reports on pigment content and spatial distribution. By isolating absorption from mixed brightfield signals, QAT enables unambiguous identification and longitudinal tracking of pigment-producing cells in a label-free manner, demonstrating its utility for functional live-cell studies. These results establish QAT as a powerful tool for melanocyte biology. Quantitative 3D mapping of melanin without exogenous labels opens new opportunities to study melanogenesis, melanosome transport, intracellular pigment organization, and population-level heterogeneity. More broadly, this work positions absorption tomography as a distinct and previously underexplored modality in biophotonics, complementing phase-based approaches and providing direct access to pathophysiologically important pigments.

The applicability of QAT to intact, optically complex tissues is further demonstrated by *in vivo* imaging of living Petunia hybrida petal cells (Fig. 4). Plant tissues pose substantial challenges due to their thickness, endogenous pigmentation, and refractive index heterogeneity. Nevertheless, QAT resolves 3D pigment distributions and captures time-resolved changes under native conditions while maintaining tissue viability. This capability extends absorption tomography from cell biology to plant biology, opening new avenues for studying pigment biosynthesis, transport, and spatial regulation in living plants.

Perhaps most importantly, QAT scales to clinically relevant human tissue specimens stained with H&E, the cornerstone of histopathological diagnosis (Fig. 5). For more than a century, hematoxylin and eosin have served as highly effective pigments for selectively staining nuclei and cytoplasm, respectively; yet pathology assessment has remained largely qualitative and two-dimensional. By reconstructing volumetric, quantitative absorption maps from standard H&E-stained sections, QAT enables 3D visualization of tissue microarchitecture with high-resolution subcellular detail that was previously inaccessible. Beyond improved visualization, the quantitative nature of QAT introduces a new dimension to histopathology. Converting H&E contrast into 3D, quantitative absorption measurements provides objective descriptors of nuclear and cytoplasmic organization that can be systematically analyzed. By converting H&E contrast into 3D, quantitative absorption maps, QAT provides a set of objective descriptors of nuclear and cytoplasmic absorption that can be systematically analyzed. While clinical validation is beyond the scope of this study, such quantitative descriptors may serve as a foundation for future efforts toward more reproducible and data-driven histopathological assessment, which can potentially reduce inter-observer variability inherent in conventional qualitative pathology.

Despite these advances, several limitations remain. QAT relies on the weak-scattering approximation and assumes absorption-dominant contrast; highly scattering or strongly refractive specimens may violate these assumptions and introduce reconstruction artifacts. Multi-illumination schemes can decouple phase and absorption contributions but increase acquisition time and computational complexity. In addition, axial resolution is ultimately constrained by the numerical aperture of the optical system and by signal-to-noise limitations inherent to absorption imaging.

Future work may address these challenges through optimized illumination strategies, advanced regularization informed by tissue priors, and hybrid reconstructions that jointly exploit absorption and refractive index information. Integration with machine learning could further enhance robustness and enable automated analysis<sup>24</sup>, including segmentation of subcellular organelles<sup>25</sup>, classification

of cell states<sup>26</sup>, and virtual staining<sup>2728</sup>. Extending QAT to chromogenic immunohistochemistry, multiplexed stains, and whole-slide imaging represents a promising direction toward 3D spatial biology and quantitative pathology<sup>3,29,30</sup>.

## Conclusion

In this work, we introduced QAT, a computational imaging framework that enables 3D, quantitative reconstruction of absorption contrast from brightfield intensity image stacks. By modeling absorption image formation in logarithmic intensity space and applying 3D deconvolution, QAT transforms stain-based brightfield microscopy from qualitative two-dimensional imaging into quantitative volumetric absorption imaging with subcellular resolution.

QAT is inherently practical: it operates on standard slide-mounted specimens, requires no interferometry or sample rotation, and is fully compatible with conventional brightfield microscope hardware combined with axial scanning. This accessibility allows quantitative 3D absorption imaging of both histochemically stained tissues and intrinsically pigmented samples without altering established workflows. By enabling volumetric, spectrally resolved absorption mapping in stained human tissue, living cells, and intact plant tissue, QAT establishes absorption tomography as a complementary imaging axis alongside phase- and fluorescence-based methods. In particular, converting chromogenic contrast into 3D quantitative measurements opens a path toward more objective and reproducible analysis of tissue architecture in histopathology.

Overall, QAT provides a physically grounded and widely deployable route to 3D absorption imaging, bridging conventional brightfield microscopy and quantitative volumetric analysis, and laying a foundation for future advances in spatial biology and quantitative pathology.

## Methods

### Imaging setup

QAT can be implemented on conventional brightfield microscopes equipped with axial scanning. In this study, we employed a custom-built brightfield transmission microscope to acquire through-focus intensity stacks under Köhler illumination. Axial scanning of the sample was used to encode 3D absorption information.

To enable programmable angular illumination and, when required, simultaneous reconstruction of absorption and refractive index, a DMD (DLP® LightCrafter™ 4500, Texas Instruments) was placed at the condenser pupil plane. The DMD generated predefined illumination patterns that controlled the pupil filling of the condenser, allowing flexible realization of both single-illumination and multi-illumination acquisition schemes.

LEDs at central wavelengths of 624 nm (red), 520 nm (green), and 455 nm (blue) (M625L4, M530L4, M455L4; Thorlabs) were used as illumination sources. The illumination was delivered to the sample through a high-numerical-aperture water-immersion condenser (UPLSAPO60XW, NA 1.2; Olympus). Transmitted light was collected by a matched 60× water-immersion objective lens (UPLSAPO60XW, NA 1.2; Olympus) and relayed onto a monochrome CMOS camera (ORX-10G-71S7M-C, Oryx; pixel size 4.5  $\mu\text{m}$ ) via an achromatic tube lens.

Axial scanning was performed using a piezoelectric translation stage (Q-545, Physik Instrumente). For large-area volumetric imaging, a motorized XY translation stage (LNR25M, Thorlabs) was used, with adjacent tiles acquired using a 25  $\mu\text{m}$  lateral overlap to facilitate stitching.

For live-cell melanocyte experiments, data were acquired using a HT platform (HT-X1, Tomocube Inc., Republic of Korea) optimized for long-term live-cell imaging. This system employs a 450 nm LED illumination source and a DMD-based structured illumination scheme, enabling acquisition protocols compatible with QAT reconstruction.

### Sample Preparation

**Calibration phantoms.** Spectrally selective absorption phantoms were prepared using cyan, magenta, and yellow (CMY) laser printer toner particles (HP 218A) and 6  $\mu\text{m}$  blue-dyed polystyrene microspheres. The particles were dispersed on glass slides and sealed with a coverslip using mounting medium. These phantoms were used to validate wavelength-specific absorption reconstruction, three-dimensional localization accuracy, and RGB composite visualization.

**Melanocyte cell culture.** B16-BL6 murine melanoma cells were cultured in standard growth medium and treated with 20  $\mu$ M forskolin to induce melanogenesis. Cells were plated on glass-bottom culture dishes and maintained at 37 °C in a humidified atmosphere with 5% CO<sub>2</sub>. For time-lapse experiments, the same field of view was repeatedly imaged over a 24 h period using a water-immersion objective to monitor melanin accumulation and redistribution.

**Petunia flower petal.** *Petunia hybrida* petals were imaged in vivo while the flower remained attached to the living plant. A single petal was gently positioned between two glass coverslips and kept hydrated throughout imaging to maintain physiological viability. The plant was returned to normal growth conditions after imaging, with no visible damage observed.

**Human pancreas tissue.** Formalin-fixed, paraffin-embedded (FFPE) human pancreatic tissue samples were sectioned to thicknesses of 10–40  $\mu$ m to preserve three-dimensional tissue architecture. Sections were stained with hematoxylin and eosin (H&E) using standard histological protocols, deparaffinized, and mounted in a refractive index-matched mounting medium. Prepared sections were placed between a glass slide and coverslip for brightfield imaging.

## Data and code Availability

The data that support the findings of this study are available from the corresponding author upon reasonable request. Custom code used for analysis and reconstruction is available from the corresponding author upon reasonable request.

## Acknowledgements

This work was supported by National Research Foundation of Korea grant funded by the Korea government (MSIT) (RS-2024-00442348, RS-2022-NR068141), Korea Institute for Advancement of Technology (KIAT) through the International Cooperative R&D program (P0028463), the Korean Fund for Regenerative Medicine (KFRM) grant funded by the Korea government (the Ministry of Science and ICT and the Ministry of Health & Welfare) (RS-2024-00332454), Commercialization Promotion Agency for R&D Outcomes (COMPA) funded by the Ministry of Science and ICT (MSIT) (RS-2024-00440577), and the Samsung Research Funding Center of Samsung Electronics under Grant (SRFC-IT1401-08).

## Competing Interests

Y.K.P. have financial interests in Tomocube Inc., a company that commercializes HT products. All other authors declare no competing interests.

## References

1. Mertz, J. C. *Introduction to Optical Microscopy*. (Cambridge university press, Cambridge New York, 2019).
2. Wang, L., Li, M. & Hwang, T. H. The 3D Revolution in Cancer Discovery. *Cancer Discov.* **14**, 625–629 (2024).
3. De Haan, K. *et al.* Deep learning-based transformation of H&E stained tissues into special stains. *Nat. Commun.* **12**, 4884 (2021).
4. Liu, Y., Levenson, R. M. & Jenkins, M. W. Slide Over: Advances in Slide-Free Optical Microscopy as Drivers of Diagnostic Pathology. *Am. J. Pathol.* **192**, 180–194 (2022).
5. Odgaard, A., Andersen, K., Melsen, F. & Gundersen, H. J. G. A direct method for fast three-dimensional serial reconstruction. *J. Microsc.* **159**, 335–342 (1990).
6. Glaser, A. K. *et al.* Light-sheet microscopy for slide-free non-destructive pathology of large clinical specimens. *Nat. Biomed. Eng.* **1**, 0084 (2017).
7. Hsieh, H.-C. *et al.* Imaging 3D cell cultures with optical microscopy. *Nat. Methods* **22**, 1167–1190 (2025).
8. Fumene Feruglio, P., Vinegoni, C., Gros, J., Sbarbati, A. & Weissleder, R. Block matching 3D random noise filtering for absorption optical projection tomography. *Phys. Med. Biol.* **55**, 5401–5415 (2010).
9. Fieramonti, L. *et al.* Time-Gated Optical Projection Tomography Allows Visualization of Adult Zebrafish Internal Structures. *PLoS ONE* **7**, e50744 (2012).
10. Holmes, T. J. & O'connor, N. J. Blind deconvolution of 3D transmitted light brightfield micrographs. *J. Microsc.* **200**, 114–127 (2000).

11. Tadrous, P. J. Subcellular Microanatomy by 3D Deconvolution Brightfield Microscopy: Method and Analysis Using Human Chromatin in the Interphase Nucleus. *Anat. Res. Int.* **2012**, 1–7 (2012).

12. Tadrous, P. J. A method of PSF generation for 3D brightfield deconvolution. *J. Microsc.* **237**, 192–199 (2010).

13. Calisesi, G. *et al.* Three-dimensional bright-field microscopy with isotropic resolution based on multi-view acquisition and image fusion reconstruction. *Sci. Rep.* **10**, 12771 (2020).

14. Kim, G. *et al.* Holotomography. *Nat. Rev. Methods Primer* **4**, 51 (2024).

15. Park, Y., Depersinge, C. & Popescu, G. Quantitative phase imaging in biomedicine. *Nat. Photonics* **12**, 578–589 (2018).

16. Streibl, N. Three-dimensional imaging by a microscope. *JOSA A* **2**, 121–127 (1985).

17. Hugonnet, H., Lee, M. J. & Park, Y. K. Quantitative phase and refractive index imaging of 3D objects via optical transfer function reshaping. *Opt. Express* **30**, 13802–13809 (2022).

18. Hugonnet, H., Lee, M. & Park, Y. Optimizing illumination in three-dimensional deconvolution microscopy for accurate refractive index tomography. *Opt. Express* **29**, 6293–6301 (2021).

19. Beck, A. & Teboulle, M. Fast Gradient-Based Algorithms for Constrained Total Variation Image Denoising and Deblurring Problems. *IEEE Trans. Image Process.* **18**, 2419–2434 (2009).

20. Jenkins, M. H. & Gaylord, T. K. Three-dimensional quantitative phase imaging via tomographic deconvolution phase microscopy. *Appl. Opt.* **54**, 9213 (2015).

21. Zuo, C. *et al.* High-resolution transport-of-intensity quantitative phase microscopy with annular illumination. *Sci. Rep.* **7**, 7654 (2017).

22. Lee, M., Shin, S. & Park, Y. Reconstructions of refractive index tomograms via a discrete algebraic reconstruction technique. *Opt. Express* **25**, 27415 (2017).

23. Bai, Z. *et al.* Absorption and phase decoupling in transport of intensity diffraction tomography. *Opt. Lasers Eng.* **156**, 107082 (2022).

24. Park, J. *et al.* Artificial intelligence-enabled quantitative phase imaging methods for life sciences. *Nat. Methods* **20**, 1645–1660 (2023).

25. Lee, M. *et al.* Deep-learning-based three-dimensional label-free tracking and analysis of immunological synapses of CAR-T cells. *Elife* **9**, e49023 (2020).

26. Kim, G. *et al.* Rapid species identification of pathogenic bacteria from a minute quantity exploiting three-dimensional quantitative phase imaging and artificial neural network. *Light Sci. Appl.* **11**, 190 (2022).

27. Jo, Y. *et al.* Label-free multiplexed microtomography of endogenous subcellular dynamics using generalizable deep learning. *Nat. Cell Biol.* **23**, 1329–1337 (2021).

28. Park, J. *et al.* Revealing 3D microanatomical structures of unlabeled thick cancer tissues using holotomography and virtual H&E staining. *Nat. Commun.* **16**, 4781 (2025).

29. Restall, B. S. *et al.* Virtual hematoxylin and eosin histopathology using simultaneous photoacoustic remote sensing and scattering microscopy. *Opt. Express* **29**, 13864 (2021).

30. Tehrani, K. F., Park, J., Chaney, E. J., Tu, H. & Boppart, S. A. Nonlinear Imaging Histopathology: A Pipeline to Correlate Gold-Standard Hematoxylin and Eosin Staining With Modern Nonlinear Microscopy. *IEEE J. Sel. Top. Quantum Electron.* **29**, 1–8 (2023).